

# Pushing the limits for medical image reconstruction on recent standard multicore processors

Jan Treibig  
Erlangen Regional Computing  
Center  
Martensstr. 1  
91058 Erlangen, Germany  
jan.treibig@rrze.uni-  
erlangen.de

Georg Hager  
Erlangen Regional Computing  
Center  
Martensstr. 1  
91058 Erlangen, Germany  
georg.hager@rrze.uni-  
erlangen.de

Hannes G. Hofmann  
Pattern Recognition Lab  
Martensstr. 3  
91058 Erlangen, Germany  
hannes.hofmann@informatik.uni-  
erlangen.de

Joachim Hornegger  
Pattern Recognition Lab  
Martensstr. 3  
91058 Erlangen, Germany  
jh@informatik.uni-  
erlangen.de

Gerhard Wellein  
Erlangen Regional Computing  
Center  
Martensstr. 1  
91058 Erlangen, Germany  
gerhard.wellein@rrze.uni-  
erlangen.de

## ABSTRACT

Volume reconstruction by backprojection is the computational bottleneck in many interventional clinical computed tomography (CT) applications. Today vendors in this field replace special purpose hardware accelerators by standard hardware like multicore chips and GPGPUs. This paper presents low-level optimizations for the backprojection algorithm, guided by a thorough performance analysis on four generations of Intel multicore processors (Harpertown, Westmere, Nehalem EX, and Sandy Bridge).

We choose the RABBITCT benchmark, a standardized test-case well supported in industry, to ensure transparent and comparable results. Our aim is to provide not only the fastest implementation but also compare to performance models and hardware counter data in order to fully understand the results. We separate the influence of algorithmic optimizations, parallelization, SIMD vectorization, and microarchitectural issues on performance and pinpoint problems with current instruction set extensions on standard CPUs (SSE, AVX). Finally we compare our results to the best GPGPU implementations available for this open competition benchmark.

## 1. INTRODUCTION AND RELATED WORK

### 1.1 CT

Computed tomography (CT) [1] is nowadays an established technology to non-invasively determine a three-dimensional

(3D) structure from a series of 2D projections of an object. Beyond its classic application area of static analysis in clinical environments the use of CT has accelerated substantially in recent years, e.g., towards material analysis or time-resolved scans supporting interventional cardiology. The numerical volume reconstruction scheme is a key component of modern CT systems and is known to be very compute-intensive. Acceleration through special-purpose hardware such as FPGAs is a typical approach to meet the constraints of real-time processing. Integrating nonstandard hardware into commercial CT systems adds considerable costs both in terms of hardware and software, as well as system complexity. From an economical view the use of standard x86 processors would be preferable. Driven by Moore's law the compute capabilities of standard CPUs have now the potential to meet the requested CT time constraints.



Figure 1: C-arm system illustration (Axiom Artis Zeego, Siemens Healthcare, Forchheim, Germany).

The volume reconstruction step for recent C-arm systems with flat panel detector can be considered as a prototype for modern clinical CT systems. Interventional C-arm CTs,



Figure 2: Volume renderings based on the 2D X-ray projections of a rabbit.

such as the one sketched in Fig. 1, perform the rotational acquisition of 496 high resolution X-ray projection images ( $1248 \times 960$  pixels) in 20 seconds [2]. This acquisition phase sets a constraint for the maximum reconstruction time to attain real-time reconstruction. In practice filtered backprojection (FBP) methods such as the Feldkamp algorithm [3] are widely used for performance reasons. The algorithm consists of 2D pre-processing steps, backprojection, and 3D post-processing. Volume data is reconstructed in the backprojection step, making it by far the most time consuming part [4]. It is characterized by high computational intensity, nontrivial data dependencies, and complex numerical evaluations but also offers an inherent embarrassingly parallel structure. In recent years hardware-specific optimization of the Feldkamp algorithm has focused on GPUs [5, 6] and IBM Cell processors [7]. For GPUs in particular, large performance gains compared to CPUs are reported [6] or documented by the standardized RABBITCT benchmark [8, 9]. Available studies with standard CPUs indicate that large servers are required to meet GPU performance [10, 11]. In this report we also use the RABBITCT environment, which defines a clinically relevant test case and is supported by industry. RABBITCT is an open competition based on C-arm CT images of a rabbit (see Fig. 2). It allows to compare the manifold of existing hardware technologies and implementation alternatives for reconstruction scenarios by applying them to a fixed, well-defined problem.

At research level recent reconstruction methods use more advanced iterative techniques, which can provide superior image quality in special cases like sparse or irregular data [12]. Other algorithms are used to reconstruct time-resolved volumes (“3D+t”) [13], e.g., for cardiac imaging. However, both approaches incorporate several backprojection steps, making performance improvements on the RABBITCT benchmark valuable for them as well. The same holds for industrial CTs in material science used in nondestructive testing (NDT), which run at higher resolution and thus further increase the computational requirements.

## 1.2 Modern processors

The steadily growing transistor budget is still pushing forward the compute capabilities of commodity processors at rather constant price and clock speed levels. Improvement and scaling of established architectural features at core level (like, e.g., SIMD and SMT; see below for details) in ad-

dition to increasing the number of cores per chip lead to peak performance levels which make standard CPUs attractive to meet the time constraints of interventional CT systems. Highly optimized single core implementations are thus mandatory for projection algorithms. Complemented by standard optimization techniques, a highly efficient SIMD (Single Instruction Multiple Data) code is the key performance component. Owing to the nontrivial data parallelism in the reconstruction scheme, SIMD optimizations need to be done at low level here, i.e., down to assembly language. However, these efforts will pay off for future computer architectures since an efficient SIMD implementation will become of major importance to further benefit from increasing peak performance numbers.

Scaling SIMD width is a safe bet to increase raw core performance and optimize energy efficiency (i.e., maximize the Flop/Watt ratio), which is known to be the critical component in future HPC systems. Recently Intel has played the game by doubling the SIMD width from the SSE instruction set (128-bit registers) to AVX [14] (256-bit registers), which is implemented in the “Sandy Bridge” architecture. More ongoing projects are pointing in the same direction, like Intel’s Many Integrated Core (MIC) [15] architecture or the Chinese Godson-3B chip [16]. Wider SIMD units do not change core complexity substantially since the optimal instruction throughput does not depend on the SIMD width. However, the benefit in the application strongly depends on the level and the structure of data parallelism as well as the capability of the compiler to detect and exploit it. For simple code patterns like streaming kernels [17] compilers are very effective, while more complex loop structures require manual intervention, at least on the level of compiler intrinsics. This is the only safe way to utilize SIMD capabilities to their full potential. The impact of wider SIMD units on programming style is still unclear since this trend currently starts to accelerate. Of course wide SIMD execution is most efficient for in-cache codes because of the large “DRAM gap.”

Simultaneous Multi-Threading (SMT) is another technology to improve core utilization at low architectural impact and energy costs. It is obvious that SMT should be most beneficial for those “in cache codes” which have limited single thread efficiency due to bubbles in arithmetic/logic pipelines, and where cache bandwidth is not the dominating factor. Naively one would not expect improvements from SMT if a code is fully SIMD vectorized since the latter technique is typically applied to simple data-parallel structures which are a paradigm for efficient pipeline use. Since many programmers do not care about pipeline occupancy in their application the benefit of SMT is often tested in an experimental way, without arriving at a clear explanation for why it does or does not help.

This paper is organized as follows. In Sect. 3 we perform a first analysis of the backprojection algorithm implemented in the RABBITCT framework using simple metrics like arithmetic throughput and memory bandwidth as guidelines for estimating performance. We address processors from four generations of Intel’s x86 processor family (Harpertown, Westmere, Nehalem EX, and Sandy Bridge). Basic optimization rules such as minimizing overall work are applied. In Sect. 4 we show how to efficiently vectorize the inner

loop kernel using SSE and AVX instructions, and discuss the possible benefit of multithreading with SMT. Sect. 5 provides an in-depth performance analysis, which will show that simple bandwidth or arithmetic throughput models are inadequate to estimate the performance of the algorithm. OpenMP parallelization and related optimizations like cc-NUMA placement and bandwidth reductions are discussed in Sect. 6. Performance results for cores, sockets, and nodes on all four platforms are given in Sect. 7, where we also interpret the effect of the different optimizations discussed earlier and validate our performance model. Finally we compare our results with current GPGPU implementations in Sect. 8.

## 2. EXPERIMENTAL TESTBED

A selection of modern Intel x86-based multi-core processors (see Table 1) has been chosen to test the performance potential of our optimizations. All of these chips feature a large outer level cache, which is shared by two (Core 2 Quad “Harpertown”), four (Sandy Bridge), six (Westmere EP), or eight cores (Nehalem EX). We refer to the maximum number of cores sharing an outer level L2/L3 cache as an “L2/L3 group.”

With the introduction of the Core i7 architecture the memory subsystem of Intel processors was redesigned to allow for a substantial increase in memory bandwidth, at the cost of introducing a ccNUMA architecture for multi-socket servers. Intel also reintroduced simultaneous multithreading (SMT, a.k.a. “Hyper-Threading”), a hardware optimization to improve the utilization of execution units. Each core supports two SMT threads. The most recent processor, Sandy Bridge, is equipped with a new instruction scheduler that supports the new AVX SIMD instruction set extension, and with a new last level cache subsystem (which was already present in Nehalem EX). The 8-core Intel Nehalem EX processor is not mainly targeted at HPC clusters but at large mission-critical servers. It reflects the performance maximum for x86 SMP nodes. A comprehensive summary of the most important processor features is presented in Table 1. Note that the Sandy Bridge model used here is a desktop variant, while the other processors are of the server (“Xeon”) type. Table 1 also contains bandwidth measurements for a simple update benchmark:

```
for(int i=0; i<N; ++i)
  a[i] = s * a[i];
```

This benchmark reflects the data streaming properties of the reconstruction algorithm and is thus better suited than STREAM [17] as a baseline for a quantitative performance model.

We use the Intel C/C++ compiler in version 12.0; since most of our performance-critical code is written in assembly language, this choice is marginal, however. Thread affinity, hardware performance monitoring, and low-level benchmarking was implemented via the LIKWID suite [18, 19], using the tools likwid-pin, likwid-perfctr, and likwid-bench, respectively.

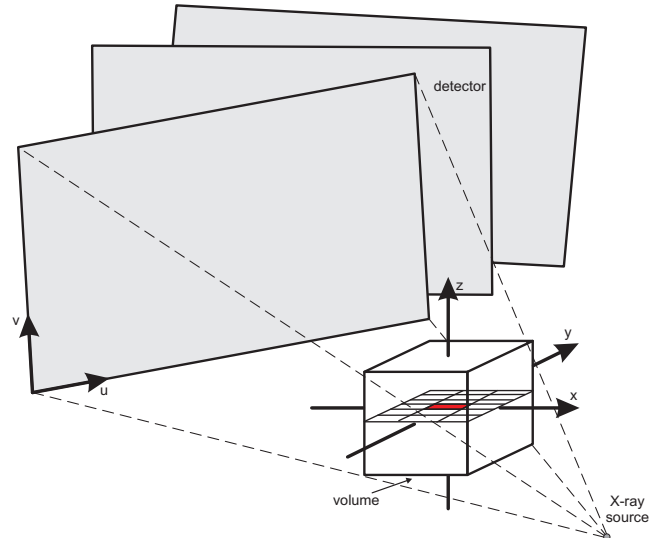


Figure 3: Setup geometry for generating the CT projection images. The size of the volume is always  $256^3 \text{ mm}^3$ , but the number of voxels may vary.

## 3. THE ALGORITHM

### 3.1 Code analysis

The backprojection algorithm (as provided by the RabbitCT framework [8], see Listing 1) is usually implemented in single precision (SP) and exhibits a streaming access pattern for most of its data traffic. One volume reconstruction uses 496 CT images (denoted by  $I$ ) of  $1248 \times 960$  pixels each ( $ISX \times ISY$ ). The volume size is  $256^3 \text{ mm}^3$ .  $MM$  is the voxel size and changes depending on the number of voxels. The most common resolution in present clinical applications is 512 voxels in each direction (denoted by the problem size  $L$ ). Each CT image is accompanied by a  $3 \times 4$  projection matrix  $A$ , which projects an arbitrary point in 3D space onto the CT image. The algorithm computes the contributions to each voxel across all projection images. The reconstructed volume is stored in array  $VOL$ . Voxel coordinates (indices) are denoted by  $x$ ,  $y$ , and  $z$ , while pixel coordinates are called  $u$  and  $v$ . See Fig. 3 for the geometric setup.

The aggregated size of all projection images is  $\approx 2.4 \text{ GB}$ . The total data transfer volume of one voxel sweep comprises the loads from the projection image and an update operation ( $VOL[i] += s$ , see line 41 in Listing 1) to the voxel array. The latter incurs 8 bytes of traffic per voxel and results (for problem size  $512^3$ ) in a data volume of 1 GB, or 496 GB for all projections. The traffic caused by the projection images is not easy to quantify since it is not a simple stream; it is defined by a “beam” of locations slowly moving over the projection pixels as the voxel update loop nest progresses. It exhibits some temporal locality since neighboring voxels are projected on proximate pixels of the image, but there may also be multiple streams with large strides. On the computational side, the basic version of this algorithm performs 13 additions, 5 subtractions, 17 multiplications and 3 divisions.

### 3.2 Simple performance models

Based on this knowledge about data transfers and arithmetic operations we can derive a first rough estimate of expected

Table 1: Test machine specifications. The cacheline size is 64 bytes for all processors and cache levels. The update benchmark results were obtained with the likwid-bench tool.

Microarchitecture	Intel Harpertown	Intel Westmere	Intel Nehalem EX	Intel Sandy Bridge
Model	Xeon X5482	Xeon X5670	Xeon X7560	Core i7-2600
Label	HPT	WEM	NEX	SNB
Clock [GHz]	3.2	2.66 (2.93 turbo)	2.26	3.4 (3.5 turbo)
Node sockets/cores/threads	2/8/-	2/12/24	4/32/64	1/4/8
Socket L1/L2/L3 cache	4×32k/2×6M/-	6×32k/6×256k/12M	8×32k/8×256k/24M	4×32k/4×256k/8M
Bandwidths [GB/s]:				
Theoretical socket BW	12.8	32.0	34.2	21.3
Update (1 thread)	5.9	15.2	3.3	16.5
Update (socket)	6.2	20.3	22.2	17.3
Update (node)	8.4	39.1	88.4	-

Listing 1: Voxel update loop nest for the plain backprojection algorithm. This gets executed for each projection  $I$ . All variables are of type `float` unless indicated otherwise. The division into parts (see text) is only approximate since there is no 1:1 correspondence to the SIMD-vectorized code.

```

1  wz = offset_z;
2  for(int z=0; z<L; z++, wz+=MM) {
3    wy = offset_y;
4
5    for (int y=0; y<L; y++, wy+=MM) {
6      wx = offset_x;
7      valtl=0.0f; valtr=0.0f;
8      valbl=0.0f; valbr=0.0f;
9
10     // Part 1 -----
11     for (int x=0; x<L; x++, wx+=MM) {
12       uw = (A[0]*wx+A[3]*wy+A[6]*wz+A[9]);
13       vw = (A[1]*wx+A[4]*wy+A[7]*wz+A[10]);
14       w  = (A[2]*wx+A[5]*wy+A[8]*wz+A[11]);
15
16       u = uw * 1.0f/w; v = vw * 1.0f/w;
17
18       int iu = (int)u, iv = (int)v;
19
20       scalx = u - (float) iu;
21       scaly = v - (float) iv;
22     // Part 2 -----
23     if (iv>=0 && iv<ISY) {
24       if (iu>=0 && iu<ISX)
25         valtl = I[iv*ISX + iu];
26       if (iu>=-1 && iu<ISX-1)
27         valtr = I[iv*ISX + iu+1];
28     }
29
30     if (iv>=-1 && iv<ISY-1) {
31       if (iu>=0 && iu<ISX)
32         valbl = I[(iv+1)*ISX + iu];
33       if (iu>=-1 && iu<ISX-1)
34         valbr = I[(iv+1)*ISX + iu+1];
35     }
36     // Part 3 -----
37     vall = scaly*valbl + (1.0f-scaly)*valtl;
38     valr = scaly*valbr + (1.0f-scaly)*valtr;
39     fx   = scalx*valr + (1.0f-scalx)*vall;
40
41     VOL[z*L*L + y*L + x] += 1.0f/(w*w)*fx;
42   } // x
43 } // y
44 } // z

```

upper performance bounds. The arithmetic limitation results in 21 cycles per vectorized update (4 and 8 inner loop iterations for SSE and AVX, respectively), assuming full vectorization and a throughput of one division per cycle. This takes into account that all architectures under consideration can execute one addition and one multiplication per cycle, neglects the slight imbalance of additions versus multiplications, and assumes that the pipelined `rcpps` instruction can be employed for the divisions (see Sect. 4.1 for details).

On the other hand, runtime can also be estimated based on the data transfer volume and the maximum data transfer capabilities of the nodes measured with the synthetic update benchmark described in Sect. 2. The following table shows lower runtime bounds for a full  $512^3$  reconstruction based on arithmetic and bandwidth limitations on the four systems in the testbed:

	HPT	WEM	NEX	SNB
Arithmetic lim. [s]	13.7	9.9	4.8	12.5
Bandwidth lim. [s]	63	13.6	6	31

The low arithmetic limitation for the single socket Sandy Bridge is caused by its wide AVX vector size and its faster clock. While above predictions seem to indicate a strongly memory-bound situation, they are far from accurate: The runtime is governed by the number of instructions and the cycles it takes to execute these instructions. A reduction to the purely “useful” work, i.e., to arithmetic operations, can not be made since this algorithm is nontrivial to vectorize due to the scattered load of the projection image and therefore involves many more nonarithmetic instructions (see Sect. 4.1 for details). We will show later that a more careful analysis leads to a completely different picture, and that further optimizations can change the bottleneck analysis considerably.

In order to have a better view on low-level optimizations we divide the algorithm into three parts:

1. Geometry computation: Calculate the index of the projection of a voxel in pixel coordinates
2. Load four corner pixel values from the projection image

- Interpolate linearly for the final update of the voxel data

### 3.3 Algorithmic optimizations

The first optimizations for a given algorithm must be on a hardware-independent level. Beyond elementary measures like moving invariant computations out of the inner loop body and reducing the divisions to one reciprocal, a main optimization is to minimize the workload. Voxels located at the corners and edges of the volume are not visible on every projection, and can thus be “clipped off” and skipped in the inner loop. This is not a new idea, but the approach presented here improves the work reduction from 24% [10] to nearly 39%.

We precompute the geometry, i.e., the position of the first and the last relevant voxel for each projection image and line of voxels (inner loop level in Listing 1). This information is always the same for a given geometric setup. It can be stored and used later during the backprojection loop. Reading the data from memory incurs an additional transfer volume of  $512^2 \times 496 \times 4$  bytes=496 MB (assuming 16-bit indexing), which is negligible compared to the other traffic. The advantage of line-wise clipping is that the shape of the clipped voxel volume is much more accurately tracked than with the blocking approach described in [10].

The if conditions (lines 23 and 30 in Listing 1) that ensure correct access to the projection image involve no measurable overhead for the scalar case due to the hardware branch prediction (and they are effectively removed by the clipping optimization described above). However, for vectorized code they are potentially costly since an appropriate mask must be constructed whenever there is the possibility that a SIMD vector instruction accesses data outside the projection [10]. To remove this complication, separate buffers are used to hold suitably padded copies of the projection images, so that there is no need for vector masks. The additional overhead is far outweighed by the performance advantage for vectorized code execution. Note that a similar effect could be achieved by peeling off scalar loop iterations to make the length of the inner loop body a multiple of the SIMD vector size and ensure aligned memory access. However, this may introduce a significant scalar component especially for small problem sizes and large vector lengths.

## 4. SINGLE CORE OPTIMIZATIONS

The basic building block for all further steps is the update of a consecutive line of voxels, which we refer to as the “line update kernel.” The baseline is an implementation in C with all optimizations from Sect. 3.3 applied.

The performance of present processors on the core level relies on instruction-level parallelism (ILP) by pipelined and superscalar execution, and data-parallel operations (SIMD). We also regard simultaneous multithreading (SMT) as a single core optimization since it is a hardware feature to increase the efficiency of the execution units by filling pipeline bubbles with useful work: The idea is to duplicate parts of the hardware resources in order to allow a quasi-simultaneous execution of different threads while sharing other parts like, e.g., floating-point ALUs. In a sense this is an alternative to outer loop unrolling, which can also

provide multiple independent instruction streams to enable a more efficient utilization of the ALUs, but is often prohibited on x86 processors because of the limited number of registers.

### 4.1 SIMD vectorization

No current compiler is able to efficiently vectorize the back-projection algorithm, so we have implemented the code directly in x86 assembly language. Using SIMD intrinsics could ease the vectorization but adds some uncertainties with regard to register scheduling and hence does not allow full control over the instruction code. All data is aligned to enable packed and aligned loads/stores of vector registers (16 (SSE) or 32 (AVX) bytes with one instruction).

The line update kernel operates on consecutive voxels. Part 1 of the algorithm (see Sect. 3.2) is straightforward to vectorize, since it is arithmetically limited and fully benefits from the increased register width. The division is replaced by a reciprocal. SSE provides the fully pipelined `rcpps` instruction for an approximate reciprocal with reduced accuracy compared to a full divide. This approximation is sufficient for this algorithm, and results in an accuracy similar to GPGPU implementations. The integer cast (line 18) is implemented via the vectorized hardware rounding instruction `roundps` introduced with SSE4.

Part 2 of the algorithm cannot be directly vectorized. As the pixel coordinates from step 1 are already in a vector register, the index calculation for `iv*ISX+iu` and `(iv+1)*ISX+iu` is done using the SIMD floating point units. There are pairs of values which can be loaded in one step because they are consecutive in memory: `valt1/valtr`, and `valbl/valbr`, respectively. Fig. 4 shows the steps involved to vectorize part 2 and the first linear interpolation. The conversion of the index into a general purpose register, which is needed for addressing the load of the data and the scattered pairwise loads, is costly in terms of necessary instructions. Moreover the runtime increases linearly with the width of the register, and the whole operation is limited by instruction throughput. There are different implementation options with the instructions available (see below). Finally the bilinear interpolation in part 3 is again straightforward to vectorize and fully benefits from wider SIMD registers.

We consider two SSE implementations, which only differ in part 2 of the algorithm. Version 1 (V1) converts the floating point values in the vector registers to four quadwords and stores the result back to memory (cache, actually). Single index values are then loaded to general purpose registers one by one. Version 2 (V2) does not store to memory but instead shifts all values in turn to the lowest position in the SSE register, from where they are moved directly to a general purpose register using the `cvtss2si` instruction.

### 4.2 AVX implementation

In theory, the new AVX instruction set extension doubles the performance per core. The backprojection cannot fully benefit from this advantage because the number of required instructions increases linearly with the register width in part 2 of the algorithm. For arbitrary SIMD vector lengths a hardware gather operation would be required to prevent this part from becoming a severe bottleneck.

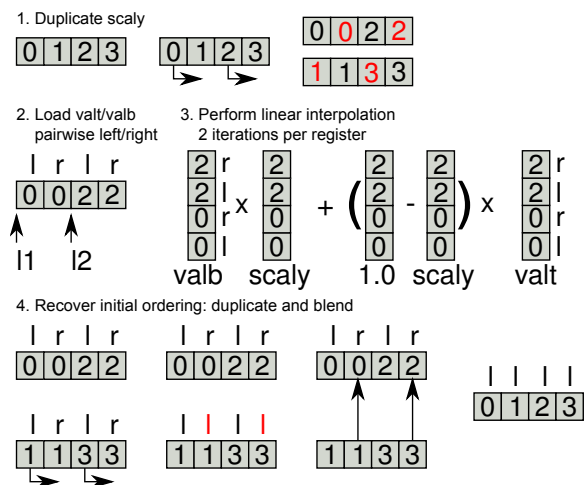


Figure 4: Vectorization of part 2 of the algorithm: The data is loaded pairwise into the vector registers. The interpolation of iterations 0,2 and 1,3 are computed simultaneously. Afterwards the results must be reordered for the second interpolation step.

Also the limited number of AVX instructions natively operating on 256-bit registers impedes more sophisticated variants of part 2; only the simple version V1 could be ported. Implementation of V2 would be possible only at the cost of a much larger instruction count, so this alternative was not considered. Still an improvement of 25% could be reached with the AVX kernel on Sandy Bridge (see Sect. 7 for detailed performance results).

### 4.3 ILP optimization and SMT

SMT can significantly improve the efficiency of the floating point units. This is especially true for cases which are limited by instruction throughput and suffer from underutilization of the arithmetic units due to dependencies or instruction scheduling issues. However, the effect of using SMT cannot be estimated quantitatively. Our measurements showed an SMT advantage of about 25% for single-socket parallel runs on Westmere and Nehalem EX (see Sect. 7 below for more complete parallel results). Sandy Bridge has a more effective instruction scheduler with less opportunity for improvement, but there is still a notable benefit of about 18%. One drawback of using SMT, the costly synchronization of threads within the same core, does not apply here.

Contrary to the first performance model, which predicted that the algorithm is memory-bound (see Sect. 3.2), we will show in Sect. 5 that the opposite is true for all processors considered here, except Harpertown.

## 5. IN-DEPTH PERFORMANCE ANALYSIS

Popular performance models for bandwidth-limited algorithms reduce the influence on runtime to the algorithmic balance, taking into account the sustained main memory performance [20]. This assumption worked well for a long time, since there was a large gap between arithmetic capabilities and main memory bandwidth. Recently it was shown [21] that this simplification is problematic on newer architectures like Intel Core i7 because of their exceptionally

large memory bandwidth per socket. E.g., a single Nehalem core cannot saturate the memory interface [22]. Moreover the additional L3 cache decouples core instruction execution from main memory transfers and generally provides a larger opportunity to overlap data traffic between different levels of the memory hierarchy. Note that in a multithreaded scenario the simple bandwidth model can indeed be used to predict performance as long as multiple cores are able to saturate the socket bandwidth. This property depends crucially on the algorithm, of course.

In [21] we have introduced a more detailed analytical method for cases where the balance model is not sufficient to predict performance with the required accuracy, and the in-cache data transfers account for a significant fraction of overall runtime. This model is based on an instruction analysis of the innermost loop body and runtime contributions of cacheline transfer volumes through the whole memory hierarchy.

A useful starting point for all further analysis is the runtime spent executing instructions with data loaded from L1 cache. The Intel Architecture Code Analyzer (IACA) [23] was used to analytically determine the runtime of the loop body. This tool calculates the raw throughput according to the architectural properties of the processor. It supports Westmere and Sandy Bridge (including AVX) as target architectures. The results for Westmere are shown in the following table for the two SSE kernel variants described above (all entries except  $\mu$ OPs are in core cycles):

Port	0	1	2	3	4	5	TP	$\mu$ OPs	CP
V1	15	21	<b>24</b>	3	3	19	<b>24</b>	85	54
V2	20	<b>27</b>	16	1	1	20	<b>27</b>	85	71

Execution times are calculated separately for all six issue ports (0..5). Apart from the raw throughput (TP) and the total number of  $\mu$ OP instructions the tool also reports a runtime prediction taking into account latencies on the critical path (CP). Based on this prediction V1 should be faster than V2 on Westmere. However, the measurements in Table 2 show the opposite result. The high pressure on the load issue port (2) together with an overall high pressure on all ALU issue ports (0, 1, and 5) seems to be decisive. In V2 the pressure on port 2 is much lower, although the overall pressure on all issue ports is slightly larger.

Below we report the results for the Sandy Bridge architecture with SSE and AVX. The pressure on the ALU ports is similar, but due to the doubled SSE load performance Sandy Bridge needs only half the cycles for the loads in kernel V1. V1 is therefore faster than V2 on Sandy Bridge (see Table 2).

Port	0	1	2	3	4	5	TP	$\mu$ OPs	CP
V1	16	<b>20</b>	14	13	3	19	<b>20</b>	85	56
V2	20	<b>26</b>	9	8	1	21	<b>26</b>	85	72
V1 AVX	18	20	22	21	6	<b>30</b>	<b>30</b>	114	90

Fig. 5 shows a full analysis in which the core execution time for a complete cacheline update is based on the measured cycles from Table 2. On the three architectures with L3 cache the simplification is made that the “Uncore” part (L3 cache, memory interface, and QuickPath interconnect) runs at the

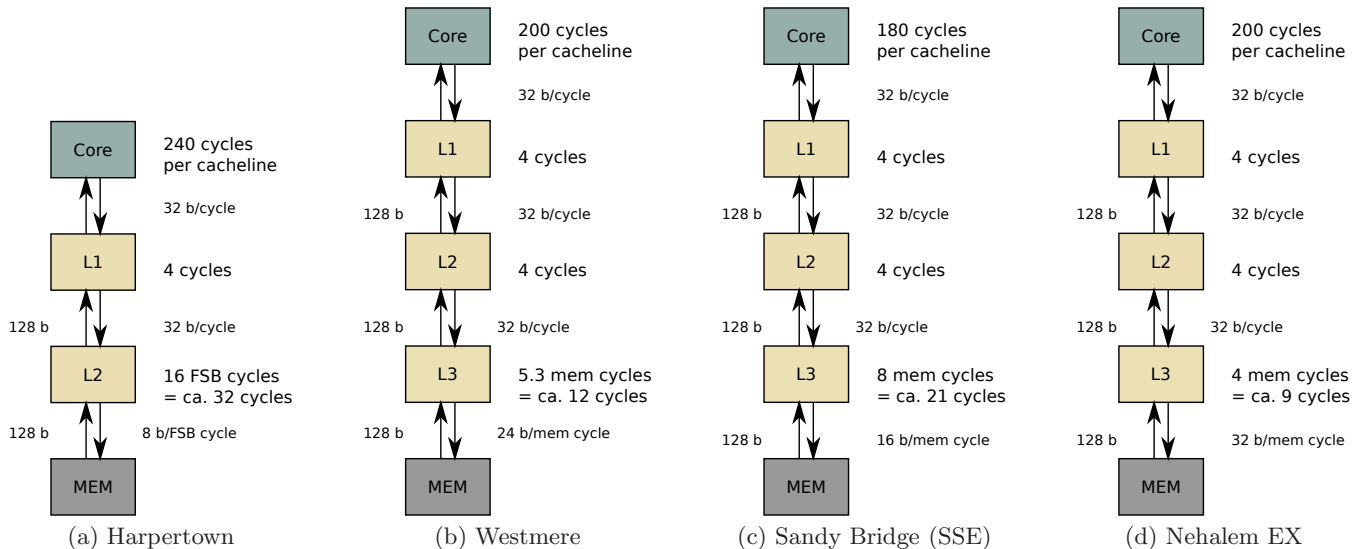


Figure 5: Performance Analysis: Runtime contributions from instruction execution and necessary cacheline transfers. Each arrow is a cacheline transfer. The total data volume in bytes is indicated on the left of each group of arrows. On the right we show the data transfer capabilities between hierarchy levels and the resulting transfer time in core cycles. For data transfers from main memory the contribution in memory/FSB cycles are translated to core cycles. In-core execution times are measured values from Table 2, scaled to a complete cacheline.

	HPT	WEM	NEX	SNB
V1	62.6	61.6	59.6	44.4
V2	57.4	51.5	54.7	50.0
V1 AVX				76.2

Table 2: Measured execution times (one core) in cycles for one iteration of the SIMD-vectorized kernel (i.e., 4 or 8 voxel updates) with all operands residing in L1 cache.

same frequency as the core, which is not strictly true but does not change the results significantly. It was shown for the Nehalem-based architectures (Westmere and Nehalem EX) that they can overlap instruction execution with reloading data from memory to the last level cache [22]. Hence, the model predicts that the in-core execution time is much larger than all other contributions, which makes this algorithm instruction throughput-limited for single core execution. On Sandy Bridge, the AVX kernel required 76.2 cycles for one vectorized loop iteration (8 updates). This results in 152 cycles instead of 180 cycles (SSE) for one cacheline update.

Based on this analysis one can estimate the total socket bandwidth and the expected runtime for one socket (we consider the full volume without clipping; bandwidths are in GB/s):

	HPT	WEM	NEX	SNB	SNB (AVX)
BW/core	1.7	1.9	1.5	2.5	3.0
BW/socket	6.8	11.2	11.6	10.0	12.0
runtime [s]	78	47	46	53	44

Comparing the required bandwidths with the measured update benchmark results in Table 1 we conclude that only Harpertown is bandwidth-limited. All other architectures are below their data transfer capabilities for this operation and should show no benefit from further bandwidth-reducing

optimizations (see Sect. 6.2).

At this point the analysis still neglects the benefit from SMT, which reduces the cycles taken for one cacheline update. The real performance values are expected to be 25% higher than predicted. A validation of the runtime prediction will be given in Sect. 7.1.

## 6. OPENMP PARALLELIZATION

OpenMP parallelization of the algorithm is straightforward and works with all optimizations discussed so far. For the thread counts and problem sizes under consideration here it is sufficient to parallelize the outer loop over all voxels (loop variable  $z$  in the listing). However, due to the clipped-off voxels at the edges and corners of the volume, simple static loop scheduling with default chunksize leads to a strong load imbalance. This can be easily corrected by using block-cyclic scheduling with a small chunksize (e.g., `static,1`).

As shown in Sect. 5, the socket-level performance analysis does not predict strong benefits from bandwidth-reducing optimizations except on the Harpertown platform. However, since one can expect to see more bandwidth-starved processor designs with more unbalanced ratio of peak performance to memory bandwidth in the future, we still consider bandwidth optimizations important for this algorithm. Furthermore, ccNUMA architectures have become omnipresent even in the commodity market, making locality and bandwidth awareness mandatory. In the following sections we will describe how to achieve proper ccNUMA page placement for voxel and image data, and how to reduce the bandwidth requirement by an effective blocking scheme. The reason why we present those optimizations in the context of shared-memory parallelization is that they become relevant only in the parallel case (see above).

## 6.1 ccNUMA placement

The reconstruction algorithm uses essentially two relevant data structures: the voxel and the image data arrays. Upon voxel initialization one can easily employ first-touch initialization, using the same OpenMP loop schedule (i.e., access pattern) as in the main program loop. This way each thread has local access (i.e., within its own ccNUMA domain) to its assigned voxel layers, and the full aggregate bandwidth of a ccNUMA node can be utilized.

Although the access to the projection image data is much less bandwidth-intensive than the memory traffic incurred by the voxel updates, ccNUMA page placement was implemented here as well. As mentioned in Sect. 3.3, the padded projection buffers are explicitly allocated and initialized in each locality domain, and a local copy is shared by all threads within a domain. Since the additional overhead for the duplication is negligible, this ensures conflict-free local access to all image data.

## 6.2 Blocking

In order to reduce the pressure on the memory interface we use a simple blocking scheme: Projections are loaded and copied to the padded projection buffers in small chunks, i.e.,  $b$  images at a time. The line update kernel (see Sect. 4) for a certain pair of  $(y,z)$  coordinates is then executed  $b$  times, once for each projection. At the problem sizes studied here, all the voxel data for this line can be kept in the L1 cache and reused  $b - 1$  times. Hence, the complete volume is only updated in memory  $496/b$  instead of 496 times. Relatively small blocking factors between 2 and 8 are thus sufficient to reduce the bandwidth requirements to uncritical levels.

This optimization is so effective that it renders proper ccNUMA placement all but obsolete; we will thus not report the benefit of ccNUMA placement in our performance results, although it is certainly performed in the code.

## 7. RESULTS

In order to evaluate the benefit of our optimizations we have benchmarked different code versions with the 512<sup>3</sup> case on all test machines. RABBITCT includes a benchmarking application, which cares of timing and error checking. It reports total runtime in seconds for the complete backprojection. We performed additional hardware performance counter measurements using the likwid-perfctr tool, which can produce high-resolution timelines of counter data and useful derived metrics on the core and node level without changes to the source code. Unless stated otherwise we always report results using SMT threads. For all architectures apart from Sandy Bridge the line update kernel version V2 was used. On Sandy Bridge results for the SSE kernel V1 as well as for the AVX port of the V1 kernel are presented.

### 7.1 Validation of analytical predictions

To validate the predicted runtime of the analytical performance model (see Sect. 5 and Fig. 5), single-socket runs were performed without the clipping optimization and SMT, but with blocking if necessary. In the following table we report the runtime and the deviation against the model prediction:

	HPT	WEM	NEX	SNB	SNB (AVX)
time	88.60	55.42	51.03	59.89	52.06
dev.	+13.6%	+17.9%	+10.9%	+13.0%	+18.3%

This shows that the model has a reasonable predictive power. It has been confirmed that the contribution of data transfers indeed vanishes against the core runtime, despite the fact that the total transfer volume is high and a first rough estimate based on data transfers and arithmetic throughput alone (Sect. 3) predicted a bandwidth limitation of this algorithm on all machines.

As a general rule, the IACA tool can provide a rough estimate of the innermost loop kernel runtime via static code analysis. Still it is necessary to further enhance the machine model to improve the accuracy of the predictions. Note that this example is an extreme case with all data transfers vanishing against core runtime. However, the approach also works for bandwidth-limited codes as was shown in [21].

### 7.2 Parallel results

Figures 6(a)–(d) display a summary of all performance results on node and socket levels, and parallel scaling inside one socket for the best version on each architecture. All machines show perfect scaling inside one socket when using physical cores only. With SMT, the benefit is considerable on Westmere and Nehalem EX, and a little smaller on Sandy Bridge, which was already shown in Sect. 4.3. The effect can be attributed to the more efficient instruction scheduler on this architecture.

Depending on the architecture, SSE vectorization boosts performance by a factor of 2–3 on the socket level. As explained earlier (see Sect. 4), part 2 of the algorithm prohibits the optimal speedup of 4 because its runtime is linear in the SIMD vector length. Work reduction through clipping alone shows only limited effect due to load imbalance, but this can be remedied by an appropriate cyclic OpenMP scheduling, as described in Sect. 6. This kind of load balancing not only improves the work distribution but also leads to a more similar access pattern to the projection images across all threads. This can be seen in Fig. 7(a), which shows the cacheline traffic between the L2 and L1 cache during a 6-thread run on one Westmere socket with all optimizations except clipping (only 3 cores are shown for clarity). Although the amount of work, i.e., the number of voxels is perfectly balanced across all threads, there is a strong discrepancy in cacheline traffic between threads when standard static scheduling is used. The reason for this is that the projections of voxel lines onto the detector are quite different for lines that are far apart from each other in the volume, which leads to vastly different access patterns to the image data, and hence very dissimilar locality properties. Cyclic scheduling removes this variation (see Fig. 7(b)).

Cache blocking has little to no effect on all architectures except Harpertown, as predicted by our analysis. Fig. 8 shows timelines for socket floating point performance and bandwidth on one Westmere socket, comparing blocked/non-blocked and SMT/non-SMT variants. Fig. 8(a) clearly demonstrates the performance boost of SMT in contrast to the very limited effect of blocking. On the other hand,

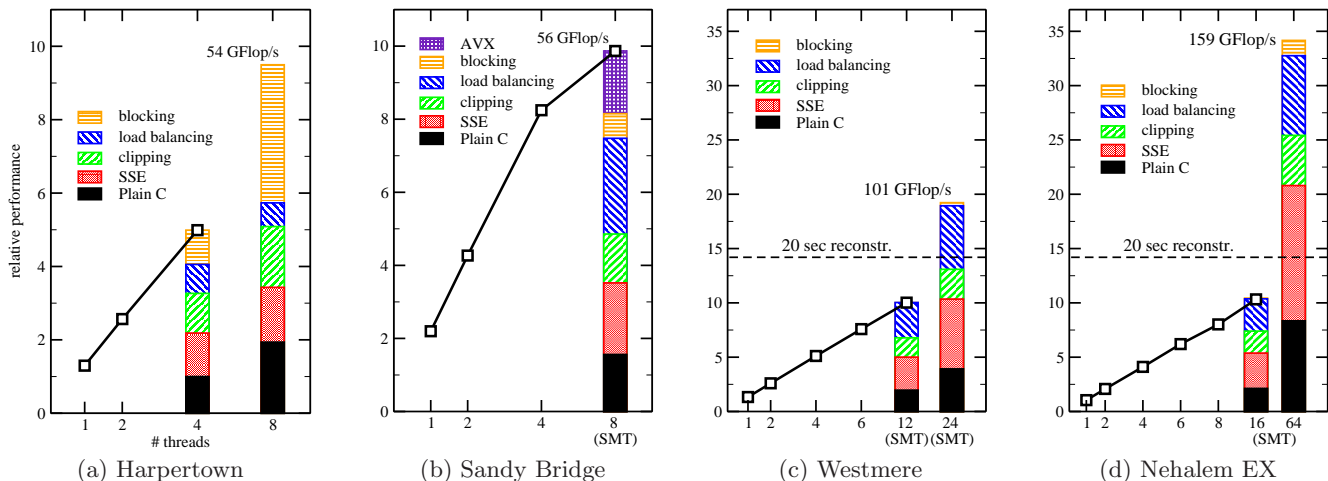


Figure 6: Scalability and performance results for the  $512^3$  test case on all platforms. Performance is normalized to the plain C code on a single Harpertown socket (4 threads). In-socket scalability was tested using the best version of the SIMD-vectorized line update kernel on each system (AVX on Sandy Bridge, SSE-V2 on all others). The practical performance goal for complete reconstruction (20 seconds runtime) is indicated as a dashed line. Note the scale change between the left and right pairs of graphs.

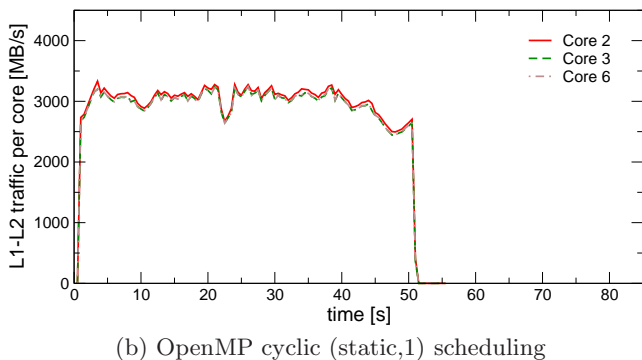
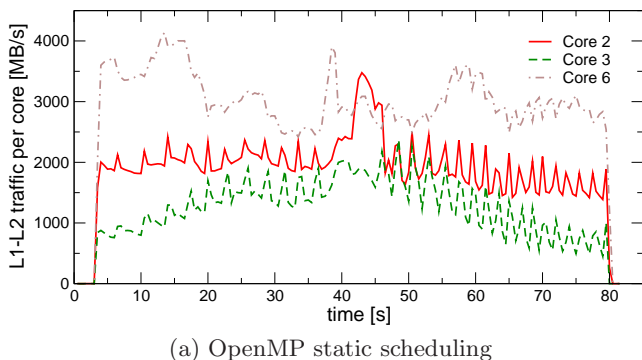


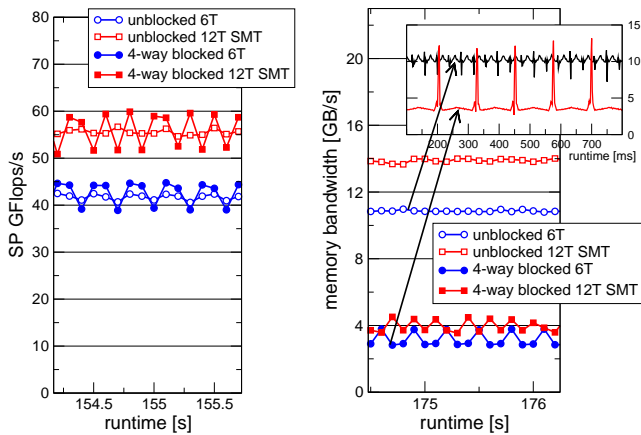
Figure 7: Timeline view of the L2 to L1 cacheline traffic for three cores of a 6-thread run without clipping on one Westmere socket, using (a) standard static OpenMP scheduling and (b) cyclic “static,1” scheduling.

the blocked implementation significantly reduces the bandwidth requirements (Fig. 8 (b)). The blocked variants have a noticeable amplitude of variations while the nonblocked versions appear smooth. In the inset of Fig. 8 (b) we show a zoomed-in view with finer time resolution, which indicates that the frequency of bandwidth variations is much larger without blocking; this is plausible since the bandwidth is dominated by the voxel volume in this case. With blocking, individual voxel lines are transferred in “bursts” with phases of inactivity in between, where image data is read at low bandwidth.

The benefit of AVX on Sandy Bridge falls short of expectations for the same reason as in the SSE case. Still it is remarkable that the desktop Sandy Bridge system outperforms the dual-socket Harpertown server node, which features twice the number of cores at a similar clock speed. Both Westmere and Nehalem EX meet the performance requirements of at most 20sec for a complete volume reconstruction. The Nehalem EX node is, however, not competitive due to its unfavorable price to performance ratio. It is an option if absolute performance is the only criterion. The Westmere node on the other hand has a price tag similar to a professional-line Nvidia Fermi card (which also requires a host system).

## 8. CPU VS. GPGPU

Since the backprojection algorithm is well suited for GPGPUs, the performance leaders of the open competition benchmark are up to now GPGPU implementations in OpenCL and CUDA. The gap to the fastest CPU version reported on the RabbitCT Web site [8] at the time of writing is very large. For the reasons given in the derivation of the performance model, simple bandwidth or peak performance comparisons are inadequate to estimate the expected reconstruction speed advantage of GPGPUs. Our implementation shows that recent x86 multicore chips are truly competitive (see Fig. 9), even when considering the price/performance



(a) FP performance (b) Memory bandwidth

Figure 8: Performance counter timeline monitoring of floating-point performance (a) and memory bandwidth (b), comparing blocked/nonblocked and SMT/non-SMT variants of the best implementation on one Westmere socket at 100 ms resolution. The inset in (b) shows a zoomed-in view with 2 ms resolution.

ratio. Beyond the clinically relevant  $512^3$  case, industrial applications need higher resolutions. This is a problem for GPGPU implementations because the local memory on the card is often too small to hold the complete voxel volume, causing extra overhead for moving partial volumes in and out of the local memory, which reduces the performance advantage even further (see the  $1024^3$  data in Fig. 9). If the price for the hardware is unimportant, a Nehalem EX node is an option that can outperform GPGPUs by far. The results for the Sandy Bridge desktop system and the good scalability even of the optimized algorithm promise even better performance levels on commodity multicore systems in the future.

Note that it would be possible to provide a simple and efficient distributed memory parallelization of the algorithm for even faster reconstruction. “Micro-clusters” based on cheap desktop technology could then easily meet any time constraint at extremely low cost.

## 9. CONCLUSIONS AND OUTLOOK

We have demonstrated several algorithmic and low-level optimizations for a CT backprojection algorithm on current Intel x86 multicore processors. Our results show that commodity hardware can be competitive with highly tuned GPU implementations for the clinically relevant  $512^3$  voxel case. At higher resolutions, which are used in industrial applications, multicore systems are frequently the only choice (apart from expensive custom solutions). Our results showed that it is necessary to consider all aspects of processor and system architecture in order to reach best performance, and that the effects of different optimizations are closely connected to each other. The benefit of the AVX instruction set on Sandy Bridge was limited due to the lack of a gathered load and the small number of instructions that natively operate on the full SIMD register width. Highly optimizing compilers were not able to deliver useful SIMD-vectorized code.

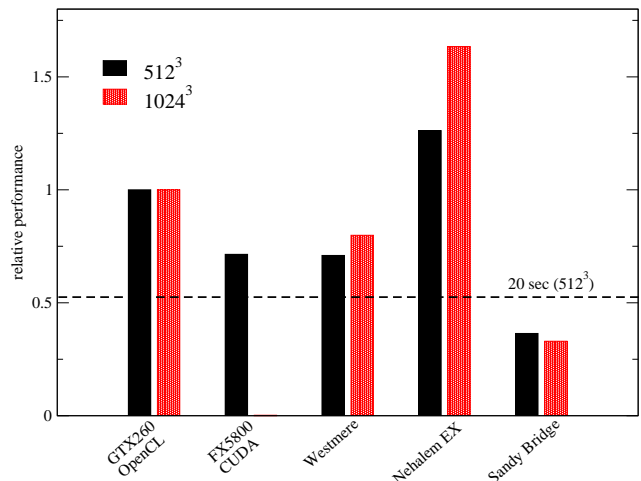


Figure 9: Performance comparison between the best reported GPGPU implementations in OpenCL and CUDA and our CPU versions on the systems in the test bed for problem sizes  $512^3$  and  $1024^3$ , respectively. There is currently no working CUDA implementation for the latter case. All performance numbers were normalized to the best GPGPU result. The practical performance goal for complete reconstruction of a  $512^3$  volume (20 seconds runtime) is indicated as a dashed line. The corresponding goal for the  $1024^3$  case with the same runtime would be at  $\approx 4.3$  in this diagram.

Future work includes a more thorough analysis and optimization of the AVX line update kernel. We also believe that there is still considerable optimization potential in current GPGPU implementations.

## 10. ACKNOWLEDGMENTS

We are indebted to Intel Germany for providing test systems and early access hardware for benchmarking. This work was supported by the Competence Network for Scientific High Performance Computing in Bavaria (KONWIHR) under project OMI4papps.

## 11. REFERENCES

- [1] A. Kak and M. Slaney. *Principles of Computerized Tomographic Imaging* (SIAM), 2001.
- [2] N. Strobel and et al. *3D Imaging with Flat-Detector C-Arm Systems*. In: *Multislice CT* (Springer, Berlin / Heidelberg), 3rd ed. ISBN 978-3-540-33125-4, 33–51.
- [3] L. Feldkamp, L. Davis and J. Kress. *Practical Cone-Beam Algorithm*. Journal of the Optical Society of America **A1(6)**, (1984) 612–619.
- [4] B. Heigl and M. Kowarschik. *High-speed reconstruction for C-arm computed tomography*. In: *9th International Meeting on Fully Three-Dimensional Image Reconstruction in Radiology and Nuclear Medicine* (www.fully3d.org, Lindau), 25–28.
- [5] K. Mueller and R. Yagel. *Rapid 3D cone-beam reconstruction with the Algebraic Reconstruction Technique (ART) by utilizing texture mapping graphics hardware*. Nuclear Science Symposium, 1998. Conference Record. **3**, (1998) 1552–1559.
- [6] K. Mueller, F. Xu and N. Neophytou. *Why do*

- Commodity Graphics Hardware Boards (GPUs) work so well for acceleration of Computed Tomography?* In: *SPIE Electronic Imaging Conference*, vol. 6498 (San Diego), 64980N.1–64980N.12.
- [7] M. Kachelrieß, M. Knaup and O. Bockenbach. *Hyperfast parallel-beam and cone-beam backprojection using the CELL general purpose hardware*. *Medical Physics* **34**(4), (2007) 1474–1486.
- [8] *RabbitCT Benchmark*. <http://www.rabbitct.com/>.
- [9] C. Rohkohl, B. Keck, H. G. Hofmann and J. Hornegger. *RabbitCT—An Open Platform for Benchmarking 3-D Cone-beam Reconstruction Algorithms*. *Medical Physics* **36**(9), (2009) 3940–3944. <http://link.aip.org/link/?MPH/36/3940/1>
- [10] H. G. Hofmann, B. Keck and J. Hornegger. *Accelerated C-arm Reconstruction by Out-of-Projection Prediction*. In: T. M. Deserno, H. Handels, H.-P. Meinzer and T. Tolxdorff (eds.), *Bildverarbeitung für die Medizin 2010* (Berlin). ISBN 978-3-642-11967-5, 380–384. <http://www5.informatik.uni-erlangen.de/Forschung/Publikationen/2010/Hofmann10-ACR.pdf>
- [11] H. G. Hofmann, B. Keck, C. Rohkohl and J. Hornegger. *Comparing Performance of Many-core CPUs and GPUs for Static and Motion Compensated Reconstruction of C-arm CT Data*. *Medical Physics* **38**(1), (2011) 3940–3944.
- [12] H. Kunze, W. Härer and K. Stierstorfer. *Iterative extended field of view reconstruction*. In: J. Hsieh and M. J. Flynn (eds.), *Medical Imaging 2007: Physics of Medical Imaging.*, vol. 6510 of *Society of Photo-Optical Instrumentation Engineers (SPIE) Conference Series* (San Diego), 65105X.
- [13] C. Rohkohl, G. Lauritsch, M. Prümmer and J. Hornegger. *Interventional 4-D Motion Estimation and Reconstruction of Cardiac Vasculature without Motion Periodicity Assumption*. In: G.-Z. Yang, D. Hawkes, D. Rueckert, A. Noble and C. Taylor (eds.), *Medical Image Computing and Computer-Assisted Intervention – MICCAI 2009*, vol. 5761 of *Lecture Notes in Computer Science* (Springer, Berlin / Heidelberg). ISBN 978-3-642-04267-6, 132–139.
- [14] Intel. *Intel advanced vector extensions programming reference*, Apr 2011.
- [15] *Intel many integrated core architecture*. <http://www.intel.com/technology/architecture-silicon/mic/index.htm>.
- [16] *Godson 3b architecture*. [http://www.theregister.co.uk/2011/02/25/ict\\_godson\\_3b\\_chip/page2.html](http://www.theregister.co.uk/2011/02/25/ict_godson_3b_chip/page2.html), Feb 2011.
- [17] *The Stream Benchmark*. <http://www.streambench.org/>.
- [18] J. Treibig, G. Hager and G. Wellein. *Likwid: A lightweight performance-oriented tool suite for x86 multicore environments*. In: *Proceedings of PSTI2010, the First International Workshop on Parallel Software Tools and Tool Infrastructures* (San Diego CA).
- [19] *LIKWID performance tools*. <http://code.google.com/p/likwid>
- [20] G. Hager and G. Wellein. *Introduction to High Performance Computing for Scientists and Engineers* (CRC Press), 2010. ISBN 978-1439811924.
- [21] J. Treibig and G. Hager. *Introducing a performance model for bandwidth-limited loop kernels*. In: *Proceedings of the Workshop Memory issues on Multi- and Manycore Platforms at PPAM 2009, the 8th International Conference on Parallel Processing and Applied Mathematics* (Wroclaw Poland). <http://arxiv.org/abs/0905.0792>
- [22] J. Treibig, G. Hager, G. and G. Wellein. *Complexities of performance prediction for bandwidth-limited loop kernels on multi-core architectures*. In: *High Performance Computing in Science and Engineering* (Springer, Berlin / Heidelberg, Garching/Munich). ISBN 978-3642138713.
- [23] Intel. *Intel architecture code analyzer*, Apr 2011. <http://software.intel.com/en-us/articles/intel-architecture>